Coupling to Charge Transfer States is the Key to Modulate the Optical Bands for Efficient Light-Harvesting in Purple Bacteria.

Lorenzo Cupellini,*,† Stefano Caprasecca,† Ciro A. Guido,† Frank Müh,§ Thomas Renger,§ and Benedetta Mennucci†

Dipartimento di Chimica e Chimica Industriale, University of Pisa, via G. Moruzzi 13, 56124, Pisa, Italy, Present Address: Verizon Connect, Via Paisiello 20, 50144 Firenze, Italy; School of Physical Sciences, The Open University, Walton Hall, Milton Keynes, MK7 6AA, United Kingdom, Present Address: Dipartimento di Scienze Chimiche, University of Padua, via F. Marzolo 1, 35131, Padova, Italy, and Institute of Theoretical Physics, Department of Theoretical Biophysics, Johannes Kepler University Linz, Altenberger Str. 69, 4040 Linz, Austria

E-mail: lorenzo.cupellini@for.unipi.it

*To whom correspondence should be addressed

†Dipartimento di Chimica e Chimica Industriale, University of Pisa, via G. Moruzzi 13, 56124, Pisa, Italy

‡Present Address: Verizon Connect, Via Paisiello 20, 50144 Firenze, Italy; School of Physical Sciences, The Open University, Walton Hall, Milton Keynes, MK7 6AA, United Kingdom

¶Present Address: Dipartimento di Scienze Chimiche, University of Padua, via F. Marzolo 1, 35131, Padova, Italy

§Institute of Theoretical Physics, Department of Theoretical Biophysics, Johannes Kepler University Linz, Altenberger Str. 69, 4040 Linz, Austria

Abstract

The photosynthetic apparatus of purple bacteria uses exciton delocalization and static disorder to modulate the position and broadening of its absorption bands, leading to efficient light harvesting. Its main antenna complex, LH2, contains two rings of identical bacteriochlorophyll pigments, B800 and B850, absorbing at 800 nm and at 850 nm, respectively. It has been an unsolved problem why static disorder of the strongly coupled B850 ring is several times larger than that of the B800 ring. Here we show that mixing between excitons and charge transfer states in the B850 ring is responsible for the effect. The linear absorption spectrum of the LH2 system is simulated by using a multi-scale approach with an exciton Hamiltonian generalized to include the charge transfer states that involve adjacent pigment pairs, with static disorder modelled microscopically by molecular dynamics simulations. Our results show that a sufficient inhomogeneous broadening of the B850 band, needed for efficient light-harvesting, is only obtained by utilizing static disorder in the coupling between local excited and inter-pigment charge transfer states.

Graphical TOC Entry

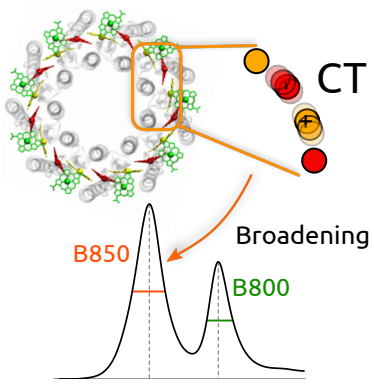

The light-harvesting apparatus of purple bacteria employs the electronic coupling between pigments to redshift absorption bands, thereby creating an excitation energy funnel, which also serves to widen its absorption spectrum. In this way, the efficiency of the system is increased, because it can absorb sunlight across a wider spectral range.

The Light-Harvesting Complex II (LH2) is a fundamental constituent of this apparatus.[1,2] Although LH2 contains several chemically identical bacteriochlorophyll *a* (BChl) pigments, it presents a characteristic spectroscopic signature with two separate absorption bands. Such spectroscopic properties are determined by the interactions among pigments, as well as the interactions between the pigments and the protein environment.[3,4] Several LH2 complexes from different bacterial species exist, all having in common the cylindrical shape and the arrangement of pigments into two rings (See Figure 1a). The rings are usually named B800 and B850 from the wavelength associated to their absorption.[1] The strong nearest-neighbor couplings among the B850 BChls make the excitation delocalized over several BChls, and ultimately determine the excited state structure of the B850 ring.[1,5] The coupling between B800 pigments is rather weak, resulting in essentially localized states and a different spectral position.[1]

Given the different excitonic characteristics of the two rings, one would expect the B850 band to be much narrower than the B800 band, due to exchange narrowing (also termed resonance energy transfer narrowing).[6–9] Instead, the B850 band is even somewhat broader than the B800 band (Figure 1c). To explain this discrepancy, simulation studies had to consider a broad inhomogeneous distribution for the site energies of B850 pigments, a factor of three to nine larger than the distribution for B800 pigments.[10–16] However, microscopic simulations have not found a wider distribution for the site energies of the B850 pigments.[5,8,17,18] The molecular origin behind this large difference has thus remained an unsolved problem that inspired the present work.

There is evidence from spectroscopy[9,19–22] and from quantum chemical calculations[23–26] that the exciton states of the B850 ring in LH2 mix with interpigment charge transfer (CT)

states, and this mixing affects their energy.[25,26] The interaction with charge-transfer states relies on interpigment wavefunction overlap, which depends exponentially on the interpigment distance. This exponential distance dependence could also be the key to understand the increased static disorder of the B850 states: mixing with CT states should strongly depend on the molecular conformation of the complex, thereby introducing large variations in the energies of the B850 band.

Here, by using a novel computational protocol, we assess the role of CT states in determining the inhomogeneous disorder of the B850 band. The present investigation demonstrates that static disorder in local excited states or long-range excitonic couplings of the B850 ring is beaten by the exchange narrowing, which leads to a strong decrease of the absorption width of the ensemble. A sufficient inhomogeneous broadening of the B850 band, needed for efficient light-harvesting, is only obtained by utilizing static disorder in the coupling between local excited and inter-pigment charge transfer states.

Being optically forbidden, CT states can only be measured indirectly, when mixed with bright states. Their exact energetic location is thus extremely difficult to pinpoint. Moreover, there is no simple model to estimate electronic coupling to CT states, unlike exciton couplings between bright states. Methods to compute couplings between CT and locally excited states exist in the literature,[27–30] but only recently studies that include those couplings in *ab initio* exciton models have been proposed.[5,25,26] Recently, some of us[26] have applied the exciton model with CT states to different spectroscopic forms of the LH2 complex of *Rbl. Acidophilus* (Formerly known as *Rps. Acidophila*[1,31]). Using a well-established multiscale polarizable quantum mechanics/molecular mechanics method (QM/MMPol) on the crystal structures of LH2, we have shown that the bright exciton state of the B850 ring is red-shifted by a different amount in the B800-B850 and B800-B820 forms of LH2.[26] Here, we exploit the structural disorder extracted from a molecular dynamics (MD) simulation of LH2 in a lipid membrane[5] to obtain coupling and energy disorder for CT states. This disorder, in turn, will reflect on the energetic disorder of exciton states and the band shape of the resulting

absorption spectrum.

The excited-state manifold of LH2 is here described in the basis of localized Q_y excitations of the 27 BChls of the complex and the 36 CT states within adjacent dimers, resulting in a 63×63 Hamiltonian matrix (See Figure 1d), whose eigenvalues E_K represent the exciton energies, whereas the eigenvectors C_{iK} represent the expansion coefficients of the exciton states $\{|K\rangle\}$ in the localized basis $\{|i\rangle\}$.

The energies and couplings among locally excited (LE) and CT states are computed along the MD using the QM/MMPol scheme, treating a BChl monomer or dimer (for B800 or B850 BChls, respectively) at the QM level, while the rest is described classically through point charges and isotropic polarizabilities. There are only two adjacent BChl dimers not related by symmetry, namely the intra-chain and inter-chain dimers (See Figure 1b). The entire LH2 system can be described with the Hamiltonian matrix elements calculated for these two dimers, together with the longer-range couplings and γ BChl energies computed in Ref. 5. All QM calculations are performed with a tuned ($\omega = 0.195$) long-range corrected[32] BLYP functional[33,34] and the 6-31G(d) basis set. Stability of the results with respect to basis sets, functionals, polarization and charge cutoffs is discussed in Section S6 of the Supporting Information.

All couplings within each dimer are computed with the multi-FED-FCD diabatization scheme devised in our previous work,[26] which combines the Fragment Excitation Difference (FED)[27] and Fragment Charge Difference (FCD)[29,35] methods. Using appropriate additional operators, the adiabatic Hamiltonian of the dimer is transformed into a diabatic basis, in order to subsequently extract the LE-LE and LE-CT couplings from the diabatic Hamiltonian matrix.[26] For each $\alpha\beta$ dimer, the excited states are combinations of the local Q_y excitations (α^* and β^*) and charge-transfer excitations ($\alpha \rightarrow \beta$ and $\beta \rightarrow \alpha$) depicted in Figure 1b. With multi-FED-FCD all energies and couplings within a dimer are obtained. The CT energies are corrected *a posteriori* with the corrected Linear Response[36] (cLR) formalism to account for the state-specific response of the environment[37–41], which is needed when a large density

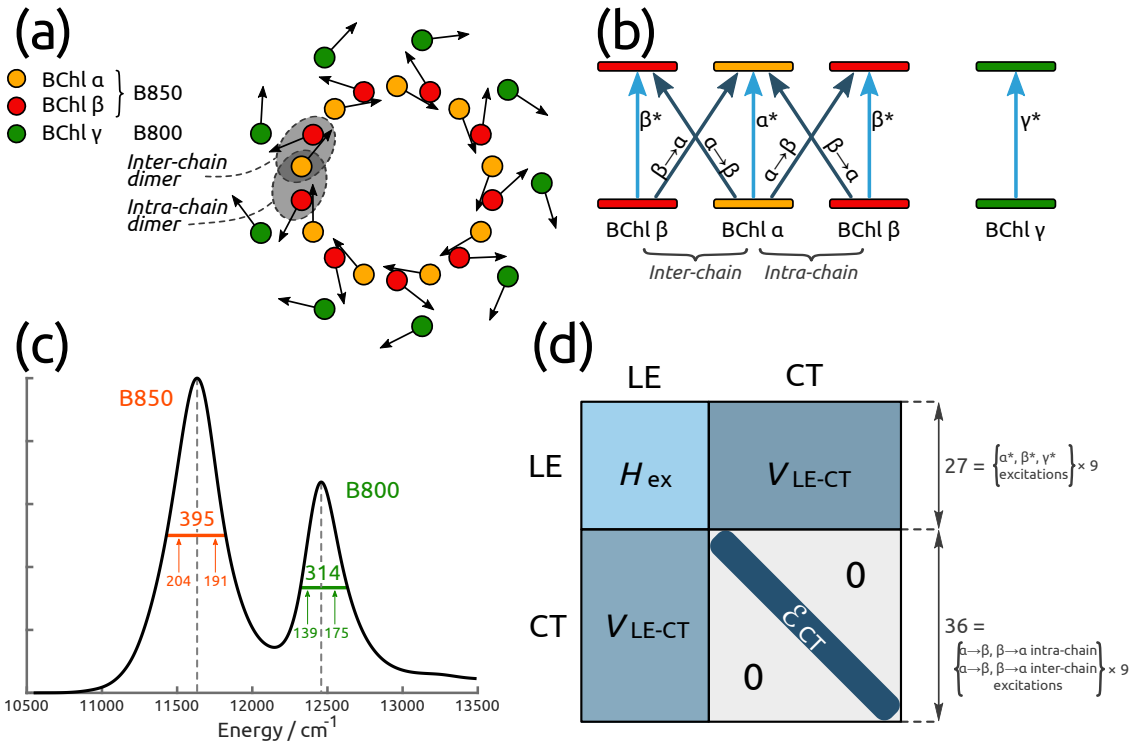

Figure 1: (a) Schematic arrangement of the BChl units in the LH2 system. The 27 BChls are divided into 9 α, 9 β (forming the B850 ring) and 9 γ (forming the B800 ring). The transition dipole moments of the Q_y transitions are shown. Adjacent ($\alpha\beta$) dimers in the B850 ring can be defined as either intra- or inter-chain. (b) Pictorial representation of the excitations considered in this work. For ($\alpha\beta$) dimers both local and charge-transfer excitations are included; the latter are considered within both inter-chain and intra-chain dimers. Local excitations of γ BChls are considered independently. The local Q_y excitations are labeled α^*, β^* and γ^*, whereas CT excitations are labeled $\alpha \rightarrow \beta$ and $\beta \rightarrow \alpha$. (c) Experimental absorption spectrum of the LH2 complex. The two excitonic peaks originating from the B850 and B800 rings are analyzed in terms of their full width at half maximum (FWHM) and their left and right components, showing a left and right skewness for B850 and B800 rings, respectively. (d) Form of the 63×63 excitonic matrix considered. LE and CT refer to the locally excited and charge transfer states included. The former comprise the Q_y state of each BChl, the latter comprise two states for inter-chain and two states for intra-chain dimers, as shown in panel B. Please see the text for explanation on the elements forming the matrix blocks.

redistribution upon excitation occurs.[42] In order to correct for uncertainties in the absolute magnitude of the quantum chemical transition density, we have rescaled all LE-LE excitonic couplings by a factor of 0.79. The latter was obtained by comparing the quantum chemical transition dipole moment of isolated BChl *a* (7.7 D) with the experimental vacuum value of 6.1 D inferred by Knox and Spring from an empty-cavity analysis of the oscillator strength

of BChl *a* in different solvents.[43]

The resulting coupling and energy distributions are summarized in Table 1 and Figure 2. Note that the signs of the couplings have been defined so that $V(\alpha^*,\beta^*)$ is positive and consistent with the dipole directions shown in Figure 1b. The site energies of α and β BChls are very close, as also noted in our previous work.[5] However, nearest-neighbor exciton couplings are lower than the ones computed there, where no correction for the transition density was applied. Nonetheless, the coupling fluctuations are almost identical to those obtained in Ref. 5.

As one can expect, CT coupling fluctuations are generally very large: the standard deviation is indeed of the same order of magnitude as the coupling average. On the contrary, excitonic couplings present much smaller fluctuations. This is due to the different distance dependence (R^{-3} versus e^{-bR}) of the excitonic and CT couplings, respectively. Nonetheless, all of these fluctuations may be important in determining the energetic disorder within the B850 band.

The energies and electronic couplings are sometimes strongly (anti)correlated within a dimer (the correlation coefficients are reported in Table S3 in the SI). This is particularly true for the two CT energies, the two electron transfer couplings, and the two hole transfer couplings, the latter four showing correlation coefficients larger than 0.95. The correlation is generally high among couplings (coefficients > 0.56 in absolute value) and negligible between couplings and energies. The correlations between states that belong to different dimers are negligible.

The presence of correlations between couplings is not surprising, since all couplings increase when reducing the inter-pigment distance. Moreover, the two hole transfer (HT) couplings, $V(\alpha^*,\alpha \rightarrow \beta)$ and $V(\beta^*,\beta \rightarrow \alpha)$, are related to the same matrix elements of the Fock operator between the HOMO orbitals of α and β.[25,44] Analogously, the two electron transfer (ET) couplings, $V(\alpha^*,\beta \rightarrow \alpha)$ and $V(\beta^*,\alpha \rightarrow \beta)$ are related to the Fock matrix element between the two LUMO orbitals. This is reflected into almost perfect correlations

($|R| > 0.95$) between these coupling pairs.

Table 1: Labels, average values and standard deviations (σ) of some energies and couplings, obtained from the sampling over 150 uncorrelated snapshots. The labels reflect the parameter characters: LE (local excitation), CT (charge transfer excitation), XT (exciton transfer coupling), ET (electron transfer coupling), HT (hole transfer coupling), see Figure 1.

		Inter-chain dimer		Intra-chain dimer	
Parameter	Label	Average / cm^{-1}	σ / cm^{-1}	Average / cm^{-1}	σ / cm^{-1}
$E(\alpha^*)$	LE1	12 585	432		
$E(\beta^*)$	LE2	12 528	446		
$E(\alpha \rightarrow \beta)$	CT1	17 179	1 538	17 727	1 605
$E(\beta \rightarrow \alpha)$	CT2	18 123	1 460	19 067	1 401
$V(\alpha^*,\beta^*)$	XT	211	53	235	33
$V(\alpha^*,\alpha \rightarrow \beta)$	ET1	−399	233	−170	156
$V(\alpha^*,\beta \rightarrow \alpha)$	HT1	−420	171	−107	113
$V(\beta^*,\alpha \rightarrow \beta)$	HT2	363	165	108	119
$V(\beta^*,\beta \rightarrow \alpha)$	ET2	475	236	162	150

The CT energies and couplings thus computed were used to expand the LH2 exciton Hamiltonian[5] as shown in Figure 1d. In order to simulate the exciton spectra, we used the disordered exciton model, where the matrix elements of the exciton Hamiltonian are sampled over a Gaussian distribution, whose average and standard deviations are those extracted from the MD and reported in Table 1; the spectra are then computed for each sample with non-equilibrium modified Redfield theory,[45] and averaged over the static disorder distribution. The exciton-phonon coupling is introduced through a spectral density extracted from experiments on the B777 complex,[46] and scaled to match the reorganization energy calculated on the dynamics. Further details on the spectra calculations are presented in Section S3 of the Supporting Information.

In order to dissect and independently analyze the effect of the different static disorder contributions on the absorption spectrum, four models of increasing realism have been defined (See Table 2):

- In model **A** the CT states are not included in the Hamiltonian, and only the static

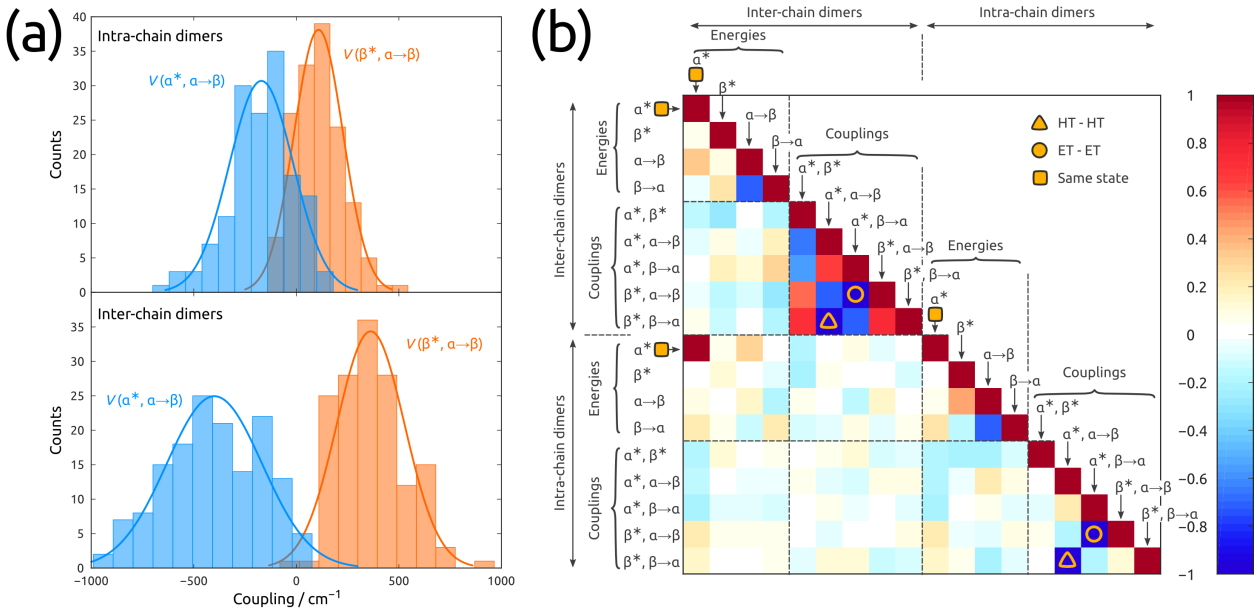

Figure 2: (a) Distributions of $V(\alpha^*,\alpha \rightarrow \beta)$ (ET) and $V(\beta^*,\alpha \rightarrow \beta)$ (HT) couplings from the snapshots considered, for both intra-chain (top) and inter-chain $\alpha\beta$ dimers (bottom). (b) Correlation coefficients among all energies and couplings considered, in inter-chain (left, top) and intra-chain dimers (right, bottom). The two strongly correlated ET-ET and HT-HT couplings are highlighted. Please note that the α^* states belonging to the inter- and intra-chain dimers (also highlighted) are actually the same state, as the dimers share an α BChl.

disorder in site energies (diagonal disorder) is considered;

- In model **B** the CT states are also included in the Hamiltonian, but only diagonal fluctuations are considered for the locally excited states (as in model **A**) and for the CT states.

- In model **C** the fluctuations of nearest-neighbor excitonic couplings and LE-CT couplings are additionally included.

- Finally, in model **D**, all the correlations were taken into account, both those between couplings (excitonic and CT) and those between the CT energies.

The absorption spectra computed with the four models are shown in Figure 3a, along with the respective FWHM and band asymmetry. Model **A** predicts a B850 band that is much narrower than the B800 band, as expected from exchange narrowing effects, and perfectly

Table 2: Definition of the disorder models

Model	Site disorder	CT states	Coupling disorder	Correlations
A	✓			
B	✓	✓		
C	✓	✓	✓	
D	✓	✓	✓	✓

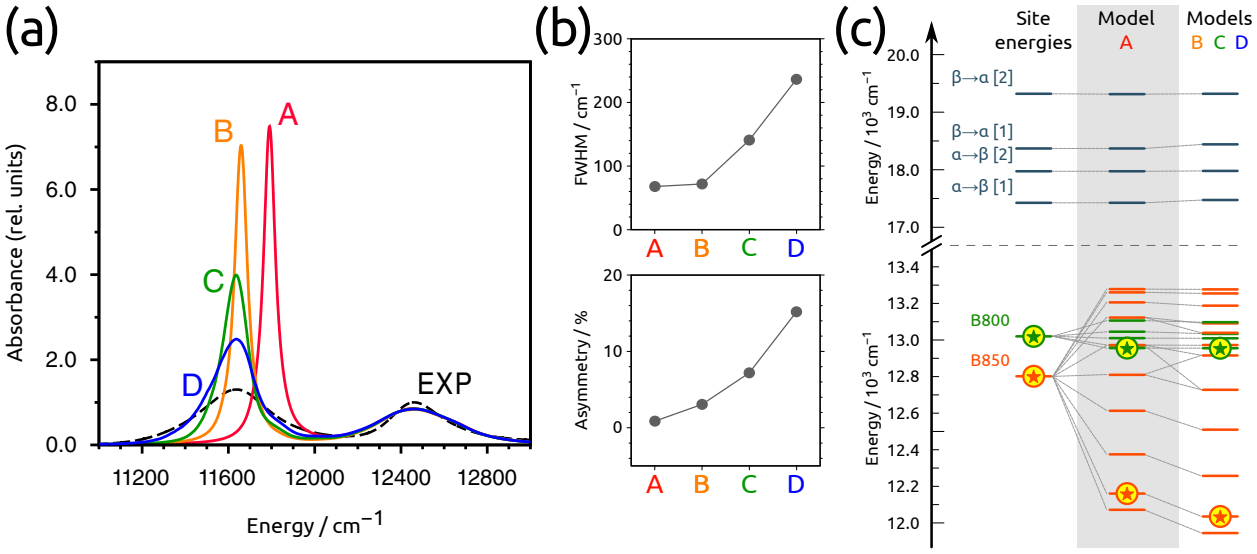

Figure 3: (a) B850 band of the LH2 absorption spectrum computed following the disorder models **A** – **D** summarized in Table 2, compared to the experimental spectrum at 300K.[5] Note that all computed spectra are shifted by -500 cm^{-1} to match the experimental B800 peak. (b) full-width at half maximum (FWHM, top) and the asymmetry (bottom) of the B850 band as a function of the model employed. The asymmetry is defined as $100 \times (w_L - w_R)/(w_L + w_R)$, where w_L and w_R are respectively the left and right widths at half maximum (c) Energy levels of the (nondisordered) locally excited and charge transfer states at various interaction models. Left: site energies of uncoupled BChl units; mid: coupling included between local excitations, as in Model **A**; right: coupling included between all states, including CT ones, as in Models **B**, **C** and **D**. Note the different scales for the LE and CT manifolds. The star signs indicate the position of the bright states.

symmetric. This result agrees with atomistic modelling studies which have not included ad-hoc inhomogeneous broadening for the B850 pigments.[8,18] The inclusion of CT states in model **B** red-shifts the B850 band by 135 cm^{-1}, due to the mixing with CT states, which are much higher in energy. The effect of CT mixing is different for the various B850 exciton states (see Figure 3c). The purely excitonic B850 states of model **A** are the eigenstates of a homogeneous ring, with increasing angular momentum, denoted by the quantum number

k. In the lower states of the ring, the couplings to the CT states all sum in phase, whereas they cancel each other in the states at the blue edge of the band.[26] For this reason, the lower-energy states are more strongly affected by the CT mixing. The B850 dipole strength is concentrated in the second exciton state, that is, the doubly degenerate $k = \pm 1$ state of the ring, which is strongly red-shifted by CT mixing. Despite the CT mixing, the broadening of the band is identical to that of model **A** (see Figure 3b), even though the disorder in the CT energies is much larger than that in the Q_y energies. In fact, CT states are only slightly mixed to exciton states (at most 2%), so the CT energy fluctuations do not significantly affect the eigenstate fluctuations, but mainly cause a red shift of the eigenstates.

Passing to model **C**, which introduces off-diagonal disorder, we see a substantial (70 cm^{-1}) broadening of the B850 band and an increase in the asymmetry. In particular, the left side of the band is some 3% larger than the right side, whereas opposite skewness is obtained for the B800 band, in qualitative agreement with the experimental data. Finally, the correlations between Hamiltonian matrix elements introduced in model **D** enhance both FWHM and asymmetry. The B850 band becomes 3.3 times wider than in models **A** and **B**. Model **D** dramatically improves the band broadening and shape, without introducing ad-hoc parameters for the disorder. The still present discrepancy with experiment, however, suggests that additional mechanisms might be active in the B850 band, which enhance energetic disorder. For example, there are CT states between second-nearest neighbors, which are higher in energy than those considered in this work, but might also contribute to the disorder. In addition, although our MD simulation is well equilibrated within 100 ns,[5] it cannot describe very slow conformational changes of LH2, that is, those occurring on the microsecond timescale or slower. This large-scale, slow conformational disorder might have additional impact on the coupling distributions and their correlations. These slow conformational degrees of freedom can be sampled, *e.g.*, by Monte Carlo techniques.[47]

Another possible reason for the too narrow lineshape of the calculated B850 band is the neglect, in the present lineshape theory, of dynamic localization effects, also known as exci-

ton self trapping,[48,49] which increase the exciton-vibrational coupling and the homogeneous broadening of the optical transitions. Hole-burning experiments on LH2 complexes have revealed the presence of exciton transitions with weak and strong exciton-vibrational coupling, corresponding to apparent Huang-Rhys factors $S = 0.3$ and $S \leq 0.8$ in the low energy wing of the B850 band.[49] The present lineshape theory reveals only the former transitions (Section 7.1 in the Supporting Information). As discussed in detail in the SI, due to the coupling of exciton states and CT states, there is a correlation between the apparent Huang-Rhys factor and the red-shift of the exciton state. The largest apparent Huang-Rhys factor of 0.25 is obtained in model **D** (including the complete coupling to CT states) at the lowest exciton transition energy (Figure S9 in the SI), in good agreement with the hole-burning data on the weakly coupled states. Including exciton-self trapping effects in the lineshape theory should reveal also the transitons with strong exciton-vibrational coupling and, hence, should further improve the agreement between experimental and calculated band widths of the B850 band.

In order to analyze the broadening mechamism, in Figure 4a we compare the distribution of exciton energies and dipole strengths for models **A** and **D**. The exchange narrowing effect in model **A** is evident for the lowest exciton states of the B850 band, whose energy distribution is much narrower than the site energy distribution. In model **D**, the CT coupling disorder lifts the symmetry constraints, allowing mixing between symmetry states, and redistributing dipole strength from the $k = \pm 1$ states to the darker states. In particular, the $k = 0$ state gains dipole strength up to $\sim$3 times the single BChl. A brighter $k = 0$ state is responsible for the observed asymmetry of the B850 band.

Figures 4b,c show how the dipole strength of the exciton states depends on the energy and delocalization length. The latter can be defined on the basis of the exciton coefficients, as the inverse participation ratio (IPR):

$$\mathrm{IPR}_K = \left(\sum_{i=1}^{N} c_{iK}^4 \right)^{-1} \tag{1}$$

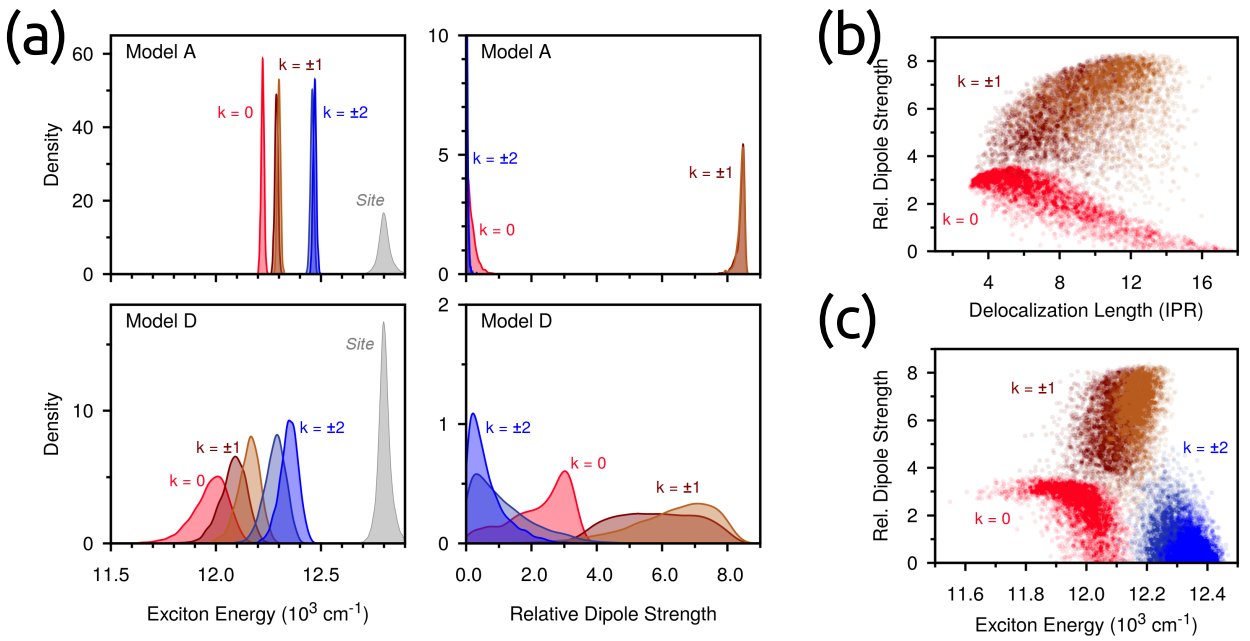

Figure 4: Statistics of exciton energy and dipole strength for the lowest exciton states of LH2. (a) Distribution of exciton energy (left) and exciton dipole strength (right) for the five lowest exciton states of LH2. Results of models **A** (top) and **D** (bottom) are compared. Note the different y-axis scale in the plots. The B850 site energy distribution is shown in grey; note that this is the same distribution in models **A**–**D**. The dipole strength is relative to the single BChl. (b) Relationship between the delocalization length (IPR) and the dipole strength for the lowest $k = 0$ and $k = \pm 1$ exciton states. (c) Relationship between the exciton energy and the dipole strength for the lowest five exciton states.

where c_{iK} is the coefficient of site i in exciton state K. IPR_K values range from one, when state K is completely localized on one site, to N, when all squared coefficients c_{iK}^2 are the same; the IPR is thus a good measure of the delocalization length. The delocalization length of state $k = 0$ reduces significantly from the maximum value of 18 down to ∼4, raising the dipole strength to that of ∼3 BChls. At the same time, the localization of the $k = \pm 1$ states on ∼4 to ∼8 pigments reduces the dipole strength of these states. In addition, state $k = 0$ acquires dipole strength when it is more red-shifted (Figure 4c): this causes the $k = 0$ state to be more emissive when it is red shifted by disorder and coupling to CT states.

The above analysis points to the (correlated) disorder in CT couplings as the main source of broadening for the B850 band. This broadening occurs through two mechanisms: firstly, fluctuations of CT couplings modulate the red-shift of the $k = \pm 1$ bright state,

thereby broadening the absorption band. Secondly, inhomogeneities in the Hamiltonian make the eigenstates deviate from those of the perfect ring, so that the dipole strength is redistributed to the neighbouring dark states.[50] For example, state $k = 0$ is essentially dark in the homogeneous ring, whereas it acquires more dipole strength the more it is localized. The large fluctuations in the Q_y-CT couplings create inhomogeneities by modulating the mixing of different B850 sites to CT states. The correlations in the fluctuations of CT couplings enhance both effects.

The energy disorder of the $k = \pm 1$ states was measured with single-molecule spectroscopy experiments, which showed that the two states have orthogonal polarization and are separated, on average, by 126 cm^{-1}.[51] These observations could be explained only by introducing correlated disorder in the site energies. Model **D** predicts mutually orthogonal polarization for states $k = \pm 1$; however, their energy separation has an average of only 77 cm^{-1} (Supporting Information, Figure S8). This discrepancy can be explained by noticing that our MD-based disorder does not include large-scale slow protein motion, which could give rise to correlated disorder (*vide supra*). Moreover, our results refer to room-temperature disorder, while single-molecule experiments are performed at very low temperatures, and the exciton structure of LH2 is sensitive to this temperature difference.[5]

The mixing with CT states can explain some spectroscopic observations on the B850 band of LH2. The increase in reorganization energy for a mixed exciton-CT state is detected as a large Huang-Rhys factor in line-narrowing spectroscopy.[9,49] In single-molecule experiments, the enhanced Huang-Rhys factors were shown to correlate with a red-shift of the band,[21] which can be attributed to an increased mixing with CT states (see Supporting Information Section 7.1). The exponential distance dependence of the CT mixing can also explain the large shift of the B850 band (as compared to the B800 band) measured under pressure.[52]

Our finding is of interest in trying to rationalize the light-harvesting strategy of purple bacteria. Efficient energy transfer among antenna complexes to the reaction center can only be achieved if there is optimal energetic alignment between the emitting states of the

donor complex and the absorbing states of the acceptor. Moreover, the absorption spectrum should be broad enough to allow for efficient light harvesting and energy funnelling. These requirements are in apparent contrast to the exciton structure of LH2, whose electronic states can be delocalized over many pigments, and most of its lowest states are optically forbidden. It is therefore not surprising that the B850 band of LH2 is much broader than expected from the exciton model, and that the $k = 0$ state is brighter. The physical explanation for this broadening and other disorder effects has been elusive for many years, and physical models have often used ad-hoc adjusted parameters to describe the disorder of the B850 band. Here instead, by employing quantum chemical calculations along a molecular dynamics of LH2 in membrane, we showed that the couplings to CT states strongly enhance its energetic disorder, contributing to most of the lineshape broadening. These results also call for additional investigation into the effect of charge-transfer mixing on the emission properties of LH2.

Supporting Information Available

Inhomogeneous width for LH2 pigments inferred from the literature. Details on quantum chemical calculations. Details on spectra simulations. Correlations among site energies and couplings. Correlation of couplings with structural parameters. Additional tests on DFT functional and rate theory. Additional disorder analysis. This material is available free of charge via the Internet at `http://pubs.acs.org/`.

References

(1) Cogdell, R. J.; Gall, A.; Köhler, J. The Architecture and Function of the Light-Harvesting Apparatus of Purple Bacteria: from Single Molecules to in Vivo Membranes. *Q. Rev. Biophys.* **2006**, *39*, 227–324.

(2) Mirkovic, T.; Ostroumov, E. E.; Anna, J. M.; van Grondelle, R.; Govindjee,; Sc-

holes, G. D. Light Absorption and Energy Transfer in the Antenna Complexes of Photosynthetic Organisms. *Chemical Reviews* **2017**, *117*, 249–293.

(3) Curutchet, C.; Mennucci, B. Quantum Chemical Studies of Light Harvesting. *Chem. Rev.* **2017**, *117*, 294–343.

(4) Renger, T.; Müh, F. Understanding Photosynthetic Light-Harvesting: a Bottom Up Theoretical Approach. *Phys. Chem. Chem. Phys.* **2013**, *15*, 3348.

(5) Cupellini, L.; Jurinovich, S.; Campetella, M.; Caprasecca, S.; Guido, C. A.; Kelly, S. M.; Gardiner, A. T.; Cogdell, R.; Mennucci, B. An Ab Initio Description of the Excitonic Properties of LH2 and Their Temperature Dependence. *J. Phys. Chem. B* **2016**, *120*, 11348–11359.

(6) Knapp, E. W. Lineshapes of Molecular Aggregates–Exchange Narrowing and Intersite Correlation. *Chem. Phys.* **1984**, *85*, 73–82.

(7) May, V.; Kühn, O. *Charge and Energy Transfer Dynamics in Molecular Systems*, 3rd ed.; Wiley-VCH Verlag GmbH: Weinheim, Germany, 2003.

(8) Olbrich, C.; Kleinekathöfer, U. Time-dependent Atomistic View on the Electronic Relaxation in Light-Harvesting System II. *J. Phys. Chem. B* **2010**, *114*, 12427–37.

(9) Rätsep, M.; Pajusalu, M.; Linnanto, J. M.; Freiberg, A. Subtle Spectral Effects accompanying the Assembly of Bacteriochlorophylls into Cyclic Light Harvesting Complexes Revealed by High-Resolution Fluorescence Spectroscopy. *J. Chem. Phys.* **2014**, *141*, 155102.

(10) van Oijen, A.; Ketelaars, M.; Kohler, J.; Aartsma, T.; Schmidt, J. Spectroscopy of Individual Light-Harvesting 2 Complexes of *Rhodopseudomonas Acidophila*: Diagonal Disorder, Intercomplex Heterogeneity, Spectral Diffusion, and Energy Transfer in the B800 Band. *Biophys. J.* **2000**, *78*, 1570–1577.

(11) Cheng, Y.; Silbey, R. Coherence in the B800 Ring of Purple Bacteria LH2. *Phys. Rev. Lett.* **2006**, *96*.

(12) Georgakopoulou, S.; Frese, R. N.; Johnson, E.; Koolhaas, C.; Cogdell, R. J.; van Grondelle, R.; van der Zwan, G. Absorption and CD Spectroscopy and Modeling of Various LH2 Complexes from Purple Bacteria. *Biophys. J.* **2002**, *82*, 2184–2197.

(13) Novoderezhkin, V. I.; Wendling, M.; Grondelle, R. V. Intra- and Interband Transfers in the B800 - B850 Antenna of *Rhodospirillum molischianum*: Redfield Theory Modeling of Polarized Pump - Probe Kinetics. *J. Phys. Chem. B* **2003**, *107*, 11534–11548.

(14) Urboniene, V.; Vrublevskaja, O.; Gall, A.; Trinkunas, G.; Robert, B.; Valkunas, L. Temperature Broadening of LH2 Absorption in Glycerol Solution. *Photosynth. Res.* **2005**, *86*, 49–59.

(15) Rancova, O.; Sulskus, J.; Abramavicius, D. Insight into the Structure of Photosynthetic LH2 Aggregate from Spectroscopy Simulations. *J. Phys. Chem. B* **2012**, *116*, 7803–7814.

(16) Segatta, F.; Cupellini, L.; Jurinovich, S.; Mukamel, S.; Dapor, M.; Taioli, S.; Garavelli, M.; Mennucci, B. A Quantum Chemical Interpretation of Two-Dimensional Electronic Spectroscopy of Light-Harvesting Complexes. *J. Am. Chem. Soc.* **2017**, *139*, 7558–7567.

(17) Damjanović, A.; Kosztin, I.; Kleinekathöfer, U.; Schulten, K. Excitons in a Photosynthetic Light-Harvesting System: A Combined Molecular Dynamics, Quantum Chemistry, and Polaron Model Study. *Phys. Rev. E* **2002**, *65*, 031919.

(18) van der Vegte, C. P.; Prajapati, J. D.; Kleinekathöfer, U.; Knoester, J.; Jansen, T. L. C. Atomistic Modeling of Two-Dimensional Electronic Spectra and Excited-State Dynamics for a Light Harvesting 2 Complex. *J. Phys. Chem. B* **2015**, *119*, 1302–13.

(19) Beekman, L.; Frese, R.; Fowler, G.; Picorel, R.; Cogdell, R.; van Stokkum, I.; Hunter, C.; vanGrondelle, R. Characterization of the Light-Harvesting Antennas of Photosynthetic Purple Bacteria by Stark Spectroscopy. 2. LH2 Complexes: Influence of the Protein Environment. *J. Phys. Chem. B* **1997**, *101*, 7293–7301.

(20) Wahadoszamen, M.; Margalit, I.; Ara, A. M.; van Grondelle, R.; Noy, D. The Role of Charge-Transfer States in Energy Transfer and Dissipation Within Natural and Artificial Bacteriochlorophyll Proteins. *Nat. Commun.* **2014**, *5*, 5287.

(21) Kunz, R.; Timpmann, K.; Southall, J.; Cogdell, R. J.; Freiberg, A.; Koehler, J. Exciton Self Trapping in Photosynthetic Pigment-Protein Complexes Studied by Single-Molecule Spectroscopy. *J. Phys. Chem. B* **2012**, *116*, 11017–11023.

(22) Ferretti, M.; Hendrikx, R.; Romero, E.; Southall, J.; Cogdell, R. J.; Novoderezhkin, V. I.; Scholes, G. D.; van Grondelle, R. Dark States in the Light-Harvesting Complex 2 Revealed by Two-dimensional Electronic Spectroscopy. *Sci. Rep.* **2016**, *6*, 20834.

(23) Scholes, G.; Gould, I.; Cogdell, R.; Fleming, G. Ab Initio Molecular Orbital Calculations of Electronic Couplings in the LH2 Bacterial Light-Harvesting Complex of *Rps. Acidophila*. *J. Phys. Chem. B* **1999**, *103*, 2543–2553.

(24) Linnanto, J.; Freiberg, A.; Korppi-Tommola, J. Quantum Chemical Simulations of Excited-State Absorption Spectra of Photosynthetic Bacterial Reaction Center and Antenna Complexes. *J. Phys. Chem. B* **2011**, *115*, 5536–5544.

(25) Li, X.; Parrish, R. M.; Liu, F.; Kokkila Schumacher, S. I. L.; Martínez, T. J. An Ab Initio Exciton Model Including Charge-Transfer Excited States. *J. Chem. Theory Comput.* **2017**, *13*, 3493–3504.

(26) Nottoli, M.; Jurinovich, S.; Cupellini, L.; Gardiner, A. T.; Cogdell, R.; Mennucci, B.

The Role of Charge-Transfer States in the Spectral Tuning of Antenna Complexes of Purple Bacteria. *Photosynth. Res.* **2018**, *137*, 215–226.

(27) Hsu, C.-P.; You, Z.-Q.; Chen, H.-C. Characterization of the Short-Range Couplings in Excitation Energy Transfer. *J. Phys. Chem. C* **2008**, *112*, 1204–1212.

(28) Difley, S.; Van Voorhis, T. Exciton/Charge-Transfer Electronic Couplings in Organic Semiconductors. *J. Chem. Theory Comput.* **2011**, *7*, 594–601.

(29) Yang, C.-H.; Hsu, C.-P. A Multi-State Fragment Charge Difference Approach for Diabatic States in Electron Transfer: Extension and Automation. *J. Chem. Phys.* **2013**, *139*, 154104.

(30) Liu, J.; Zhang, Y.; Bao, P.; Yi, Y. Evaluating Electronic Couplings for Excited State Charge Transfer Based on Maximum Occupation Method ΔSCF Quasi-Adiabatic States. *J. Chem. Theory Comput.* **2017**, *13*, 843–851.

(31) Imhoff, J. F. Transfer of *Rhodopseudomonas Acidophila* to the New Genus *Rhodoblastus* as *Rhodoblastus Acidophilus* Gen. Nov., Comb. Nov. *Int. J. Syst. Evol. Microbiol.* **2001**, *51*, 1863–1866.

(32) Iikura, H.; Tsuneda, T.; Yanai, T.; Hirao, K. A Long-Range Correction Scheme for Generalized-Gradient-Approximation Exchange Functionals. *J. Chem. Phys.* **2001**, *115*, 3540–3544.

(33) Becke, A. D. Density-Functional Exchange-Energy Approximation with Correct Asymptotic Behavior. *Phys. Rev. A* **1988**, *38*, 3098–3100.

(34) Lee, C.; Yang, W.; Parr, R. G. Development of the Colle-Salvetti Correlation-Energy Formula into a Functional of the Electron Density. *Phys. Rev. B* **1988**, *37*, 785–789.

(35) Voityuk, A. A.; Rösch, N. Fragment Charge Difference Method for Estimating

Donor–Acceptor Electronic Coupling: Application to DNA π-stacks. *J. Chem. Phys.* **2002**, *117*, 5607.

(36) Caricato, M.; Mennucci, B.; Tomasi, J.; Ingrosso, F.; Cammi, R.; Corni, S.; Scalmani, G. Formation and Relaxation of Excited States in Solution: A New Time Dependent Polarizable Continuum Model Based on Time Dependent Density Functional Theory. *J. Chem. Phys.* **2006**, *124*, 124520.

(37) Cammi, R.; Corni, S.; Mennucci, B.; Tomasi, J. Electronic Excitation Energies of Molecules in Solution: State Specific and Linear Response Methods for Nonequilibrium Continuum Solvation Models. *J. Chem. Phys.* **2005**, *122*, 104513.

(38) Corni, S.; Cammi, R.; Mennucci, B.; Tomasi, J. Electronic Excitation Energies of Molecules in Solution within Continuum Solvation Models: Investigating the Discrepancy Between State-Specific and Linear-Response Methods. *J. Chem. Phys.* **2005**, *123*, 134512.

(39) Improta, R.; Barone, V.; Scalmani, G.; Frisch, M. J. A State-Specific Polarizable Continuum Model Time Dependent Density Functional Theory Method for Excited State Calculations in Solution. *J. Chem. Phys.* **2006**, *125*, 054103.

(40) Marenich, A. V.; Cramer, C. J.; Truhlar, D. G.; Guido, C. A.; Mennucci, B.; Scalmani, G.; Frisch, M. J. Practical Computation of Electronic Excitation in Solution: Vertical Excitation Model. *Chem. Sci.* **2011**, *2*, 2143–2161.

(41) Lunkenheimer, B.; Köhn, A. Solvent Effects on Electronically Excited States Using the Conductor-Like Screening Model and the Second-Order Correlated Method ADC(2). *J. Chem. Theory Comput.* **2013**, *9*, 977–994.

(42) Guido, C. A.; Jacquemin, D.; Adamo, C.; Mennucci, B. Electronic Excitations in Solution: The Interplay between State Specific Approaches and a Time-Dependent Density Functional Theory Description. *J. Chem. Theory Comput.* **2015**, *11*, 5782–5790.

(43) Knox, R.; Spring, B. Q. Dipole Strength in the Chlorophylls. *Photochem. Photobiol.* **2003**, *77*, 497–501.

(44) Madjet, M. E.-A.; Müh, F.; Renger, T. Deciphering the Influence of Short-Range Electronic Couplings on Optical Properties of Molecular Dimers: Application to "Special Pairs" in Photosynthesis. *J. Phys. Chem. B* **2009**, *113*, 12603–12614.

(45) Dinh, T.-C.; Renger, T. Lineshape Theory of Pigment-Protein Complexes: How the Finite Relaxation Time of Nuclei Influences the Exciton Relaxation-Induced Lifetime Broadening. *J. Chem. Phys.* **2016**, *145*.

(46) Renger, T.; Marcus, R. A. On the Relation of Protein Dynamics and Exciton Relaxation in Pigment-Protein Complexes: An Estimation of the Spectral Density and a Theory for the Calculation of Optical Spectra. *J. Chem. Phys.* **2002**, *116*, 9997–10019.

(47) Fokas, A. S.; Cole, D. J.; Hine, N. D.; Wells, S. A.; Payne, M. C.; Chin, A. W. Evidence of Correlated Static Disorder in the Fenna-Matthews-Olson Complex. *J. Phys. Chem. Lett.* **2017**, *8*, 2350–2356.

(48) Sumi, H. Exciton Polarons of Molecular Crystal Model. II. Optical Spectra. *J. Phys. Soc. Japan* **1975**, *38*, 825–835.

(49) Freiberg, A.; Rätsep, M.; Timpmann, K.; Trinkunas, G.; Woodbury, N. W. Self-Trapped Excitons in LH2 Antenna Complexes between 5 K and Ambient Temperature. *J. Phys. Chem. B* **2003**, *107*, 11510–11519.

(50) Novoderezhkin, V. I.; Rutkauskas, D.; van Grondelle, R. Dynamics of the Emission Spectrum of a Single LH2 Complex: Interplay of Slow and Fast Nuclear Motions. *Biophys. J.* **2006**, *90*, 2890–2902.

(51) Hofmann, C.; Aartsma, T. J.; Köhler, J. Energetic Disorder and the B850-Exciton

States of Individual Light-Harvesting 2 Complexes from Rhodopseudomonas Acidophila. *Chem. Phys. Lett.* **2004**, *395*, 373–378.

(52) Timpmann, K.; Ellervee, A.; Pullerits, T.; Ruus, R.; Sundstrom, V.; Freiberg, A. Short-range Exciton Couplings in LH2 Photosynthetic Antenna Proteins Studied by High Hydrostatic Pressure Absorption Spectroscopy. *J. Phys. Chem. B* **2001**, *105*, 8436–8444.